WELDING RESEARCH

SUPPLEMENT TO THE *WELDING JOURNAL*, MAY 1994
Sponsored by the American Welding Society and the Welding Research Council

Modeling Primary Dendrite Arm Spacings in Resistance Spot Welds Part II — Experimental Studies

Experiments on sheet steel of three different thicknesses and yield strengths verify models for predicting primary dendrite spacings

BY J. E. GOULD

ABSTRACT. Hold time sensitivity is a potential concern when cold-rolled high-strength low-alloy sheet steels are used in resistance spot welded applications. Hold time sensitivity is defined by cracking, which occurs along the faying surface of the weld on peel testing when conventional hold times are used, and does not occur when reduced hold times are used. Hold time sensitivity is related to solidification cracking in the steel; however, it is believed that steel hardenability may also play a role. As an aid to understanding of solidification cracking in resistance spot welds, it is necessary to have an understanding of how the solidification structure develops. In this work, solidification structures in resistance spot welds have been characterized by the primary dendrite spacing. In Part I of this work, primary dendrite spacings were modeled by using a combination of numerical thermal modeling and closed-form primary dendrite spacings modeling. Numerical thermal modeling was used to predict solidification conditions in these welds. These solidification conditions were then used in the primary dendrite spacings model to predict the local spacings. In this paper, experimental studies were conducted to examine the validity of the modeling described in the previous paper.

Experimentally, primary dendrite spacings were characterized for three grades of cold-rolled HSLA steel with nominal compositions of 0.05C-0.3Mn, 0.1C-1Mn and 0.15C-1.5Mn. For each steel, three separate thicknesses (nominally 0.8, 1.25 and 2.0 mm) were investigated. Primary dendrite spacings were determined at nominally the weld faying surface from deep-etched micrographs using an area-averaging technique.

Empirically, the observed primary dendrite spacings were found to increase with increasing gauge. Also, primary dendrite spacings were found to increase with increases in composition. Primary dendrite spacings in the individual steel types were found to correlate well with the predicted solidification conditions (taken from the numerical thermal model). Correlations were done between as a power relationship with either G x R or G x $R^{1/2}$. Both fits appeared equally good, and the predicted exponents in either case are consistent with other efforts in this area.

Correlations were established between primary dendrite spacing, solidification conditions and steel composition using either of two spacings models. In order to apply these models, the steels under study must have solidification events defined by a single alloy addition. A careful examination of the material and composition terms used in these models, as well as the compositions of the actual steels used, showed that solidification was dominated by C addition. As such, for the purpose of this solidification modeling, the steels were treated as essentially Fe-C binary alloys. These results indicate that the primary dendrite spacings in these welds correlate well with the predicted solidification conditions and bulk C content. Predicted exponent in the fit was very close to that predicted in either of the primary dendrite spacings models considered.

Note was taken that hold time sensi-

KEY WORDS

Resistance Spot Weld
Modeling
Dendrite Arm Spacing
Hold Time Sensitivity
HSLA
Solidification
Num. Therm. Modeling
Structural Modeling
Steel Thicknesses
Steel Composition

J. E. GOULD is with the Edison Welding Institute, Columbus, Ohio.

Table 1 — Types, Gauges and Detailed Compositions of the Steels Used in This Study

Material	Gauge (mm)	C (%)	Mn (%)	P (%)	S (%)	Si (%)	Al (%)
0.05C-0.3Mn	0.791	0.040	0.31	0.011	0.010	0.014	0.038
0.05C-0.3Mn	1.22	0.065	0.50	0.009	0.009	0.025	0.034
0.05C-0.3Mn	1.91	0.062	0.45	0.011	0.014	0.026	0.048
0.10C-1Mn	0.737	0.12	0.97	0.015	0.010	0.29	0.043
0.10C-1Mn	1.27	0.11	1.20	0.022	0.010	0.33	0.051
0.10C-1Mn	1.98	0.084	1.04	0.018	0.012	0.25	0.054
0.15C-1.5Mn	0.89	0.15	0.17	0.017	0.011	0.29	0.048
0.15C-1.5Mn	1.45	0.15	0.20	0.020	0.012	0.28	0.047
0.15C-1.5Mn	2.13	0.14	0.20	0.020	0.011	0.30	0.037

tivity generally increases with both decreasing gauge or increasing composition. However, the primary dendrite spacings apparently decrease with decreasing gauge, and increase with increasing composition. As such, hold time sensitivity does not directly correlate with primary dendrite spacing. It is believed that solidification cracking will generally increase with increasing primary dendrite spacings; however, the lighter gauges (with greater cooling rates) result in greater contractual stresses, increasing the likelihood of solidification cracking (and hold time sensitivity). To fully understand hold time sensitivity in resistance spot welds, more detailed thermomechanical modeling will be required.

Introduction

Hold time sensitivity is considered a critical aspect of resistance spot welding cold-rolled high-strength sheet steels (Refs. 1–5). Previous work has documented that a major cause of hold time sensitivity is solidification related cracking (hot cracking) (Ref. 4). This study was initiated to understand relationships between steel composition, steel gauge and susceptibility to hold time sensitivity. The basic approach has been to examine these relationships through modeling the primary dendrite spacings in resistance spot welds on a range of HSLA steels. This modeling coupled predictions of solidification conditions in spot welds taken from an existing numerical model (Ref. 4) with a closed-form solution predicting dendrite spacings as a function of these solidification conditions.

Table 2 — Welding Conditions Used for the Three Gauges of Steel under Study

Nominal Gauge (mm)	Electrode Diameter (mm)	Weld Time (cycles)	Weld Force (kN)	Weld Current (approximate) (kA)
0.8	6.4	9	2.85	8.4
1.25	7.9	13	4.45	12
2.0	7.9	21	6.36	13

Details of the modeling work were presented in Part I of this work (Ref. 6). Included in Part I were details of the numerical simulation, approaches for modeling primary dendrite spacings and details for adapting the numerical modeling results to specific spot weld geometries. Also detailed in Part I were examples of variations in solidification conditions over the freezing cycle of spot welds made on some representative gauges of steels.

In this work, solidification conditions were found to be extremely sensitive to both the gauge of the steel being welded, and the relative degree of solidification of the weld nugget. Typically, conditions following the onset of solidification (immediately after termination of the weld current) showed the highest solidification rates and steepest thermal gradients. Also, welds made on lighter gauges of steel throughout solidification of the weld nugget showed higher solidification rates and steeper thermal gradients. Based on the primary dendrite spacings modeling results presented in the prior work, increasing dendrite spacings were predicted for both the advancing solidification front and for thicker gauges of steels. Increased compositions were also inferred to result in increased primary dendrite spacings.

In this part of the work, experimental examinations were done to verify the relationships suggested by the modeling detailed in Part I. Here, primary dendrite spacings in spot welds on nine variations of steels were examined. These included three gauge variations (nominally, 0.8, 1.25 and 2.0 mm) and three composition variations (nominally 0.05%C - 0.3%Mn, 0.1%C - 1.0%Mn and 0.15%C - 1.5%Mn steels). Primary dendrite spacings for spot welds on each steel were characterized along the faying surface by careful sectioning polishing and etching. Actual primary dendrite spacings were determined from micrographs using a space fill assumption. Results were then correlated with the modeling results as detailed in Part I to determine the validity of this approach for understanding solidification structure variations, as well as their relationship to hold time sensitivity in resistance spot welds.

Experimental

In this study, three separate types of continuously annealed HSLA steels were used. These nominally conformed to classifications of 280, 350 and 560 MPa yield strength steels. To achieve these strength levels, each of these steels employed differing levels of C, Mn and Si additions. Nominal compositions for each of these steels is as follows: 280 MPa (40 ksi), 0.05C-0.3Mn; 350 MPa (50 ksi), 0.10C-1Mn-0.3Si; 560 MPa (80 ksi), 0.15C-1.5Mn-0.3Si.

In these experiments, three separate thicknesses of each steel were employed. These included thicknesses of nominally 0.8, 1.25 and 2.0 mm (0.030, 0.050 and 0.080 in.). Types, thicknesses and detailed compositions of each of the steels used are given in Table 1.

Welding was done on a 100-kVA Sciaky press-type single-point resistance spot welding machine. Welding current was monitored using a Duffers 8120 current meter. Welding conditions, including the type of electrode used, were taken from the appropriate Ford Motor Co. specification (Ref. 7). Electrodes were all of the truncated cone geometry. The lightest gauge steel (nominally 0.8 mm) used an electrode with a 6.4-mm (0.25-in.) face and a 90-deg included angle. The heavier gauge steels used an electrode with a 7.9-mm (0.31-in.) face and a 120-deg included angle. In all welding trials, electrodes were dressed and subjected to 25 break-in welds prior to any testing. Current levels for these test welds were then determined by increasing the welding current (all other process conditions remaining constant) until conditions just below expulsion were achieved. Separate trials were made for each combination of steel type and steel thickness. Actual welding conditions for each case are given in Table 2. Welds were then used for the subsequent sectioning described below.

Two sample welds from each combi-

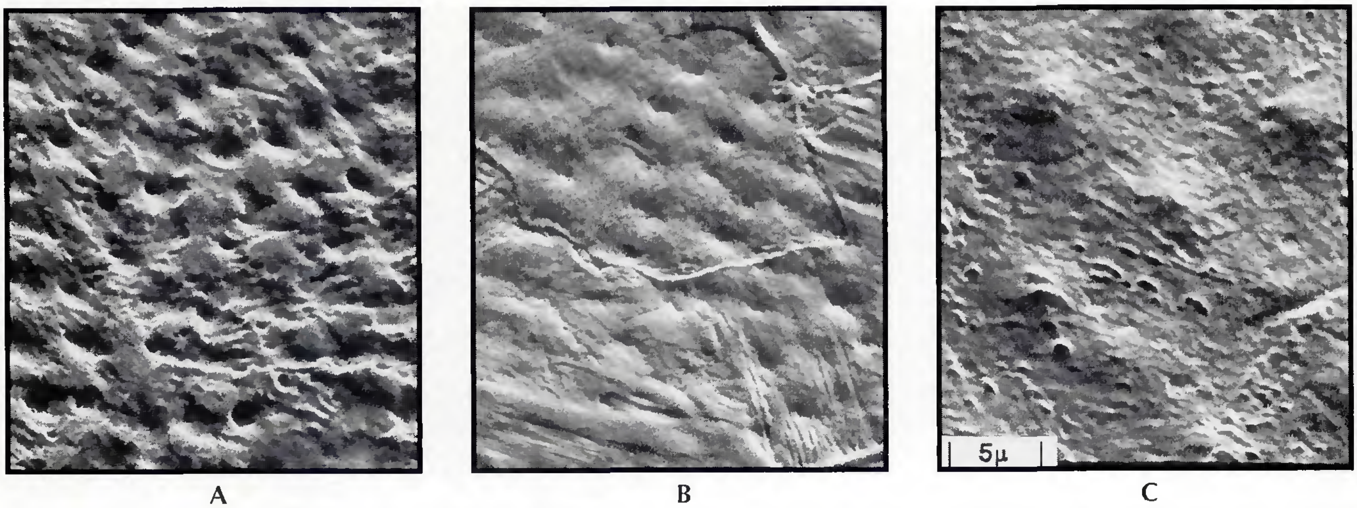

Fig. 1 — End-on dendrite morphologies for the 0.05C-0.3Mn steel spot weld. A — Nominally 0.8-mm-thick sample; B — nominally 1.25-mm-thick sample; C — nominally 2.0-mm-thick sample.

nation of material type and steel thickness were subjected to sectioning and metallurgical examination. The first was sectioned normal to the centerline or faying surface of the weld in order to reveal the degree of penetration of the weld, and any indentation of the electrodes into the sheets. The second was sectioned along the faying surface. This was used for end-on examination of the dendrite spacings. For this set of samples, the weld was sectioned slightly to one side of the parting surface of the sheets (at the faying surface). The sample was then ground back to a point just across the faying surface, polished and examined.

Following polishing, all metallographic samples were subjected to deep etching in a saturated picric acid solution. This etchant was found to be very effective in revealing solidification structures in steel welds. Resulting samples were characterized using either optical or scanning electron microscopy (SEM). SEM was used where resolution of the solidification structure was difficult. Where possible, however, optical microscopy was used.

Results

Observations of Primary Dendrite Structures

Each of the metallographic specimens used for end-on observation of the dendrites was examined with the appropriate instrument (optical microscope or SEM) for best revealing these structures. Generally, the ease with which the structures could be resolved was a function of two (probably compounded) factors; the degree of residual segregation in the structure, and the dendrite spacing itself.

The end-on solidification structures for the three thicknesses of the 0.05C-0.3Mn steel are presented in Fig. 1. Parts A, B and C of Fig. 1 represent the solidification structures for the 0.8-, 1.25- and 2.0-mm-thick steels, respectively. For these steels, the degree of residual segregation was relatively small, so SEM was required to reveal the underlying structure. The solidification structure, in this orientation and for this composition of steel, appears as an array of shallow indentations. These indentations are believed to represent interdendritic regions, however, their exact nature is not clear from the micrographs. These micrographs do indicate clearly the effect steel thickness has on the scale of the primary dendrite spacings; increasing thicknesses correspond to increasing spacings.

An interesting facet of these micrographs is the apparent washing out of the underlying microstructure. The outlines of prior austenite grains can be observed and, to some degree, relationships between the prior grain structure and primary dendrite structure can be examined. However, evidence of the

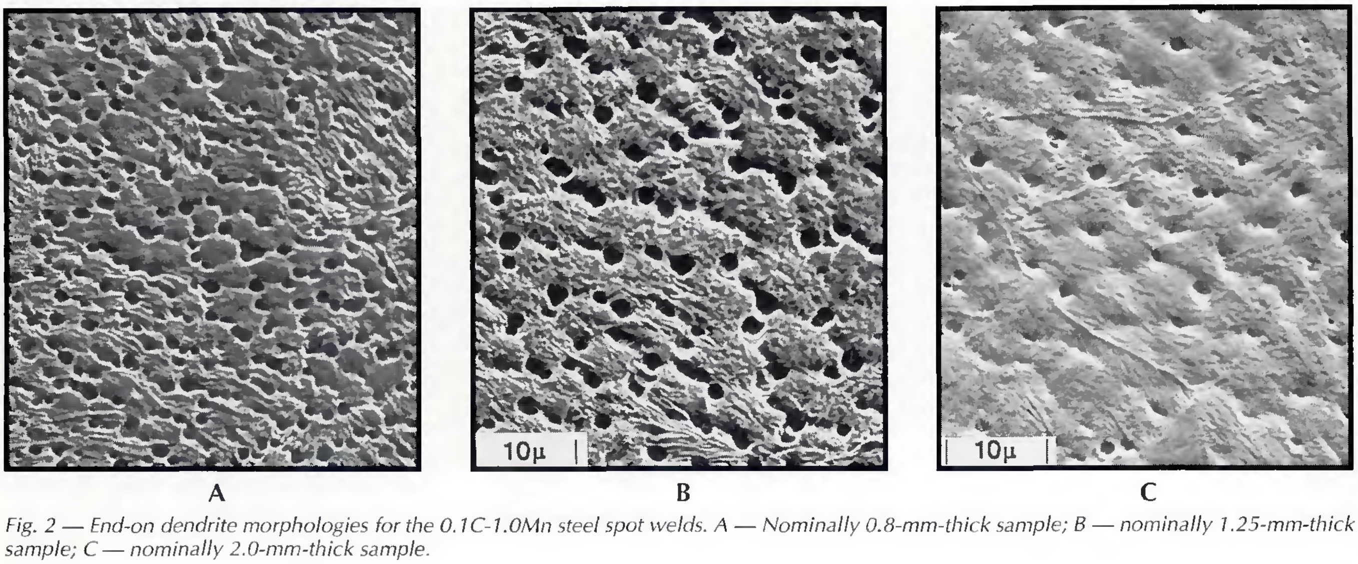

Fig. 2 — End-on dendrite morphologies for the 0.1C-1.0Mn steel spot welds. A — Nominally 0.8-mm-thick sample; B — nominally 1.25-mm-thick sample; C — nominally 2.0-mm-thick sample.

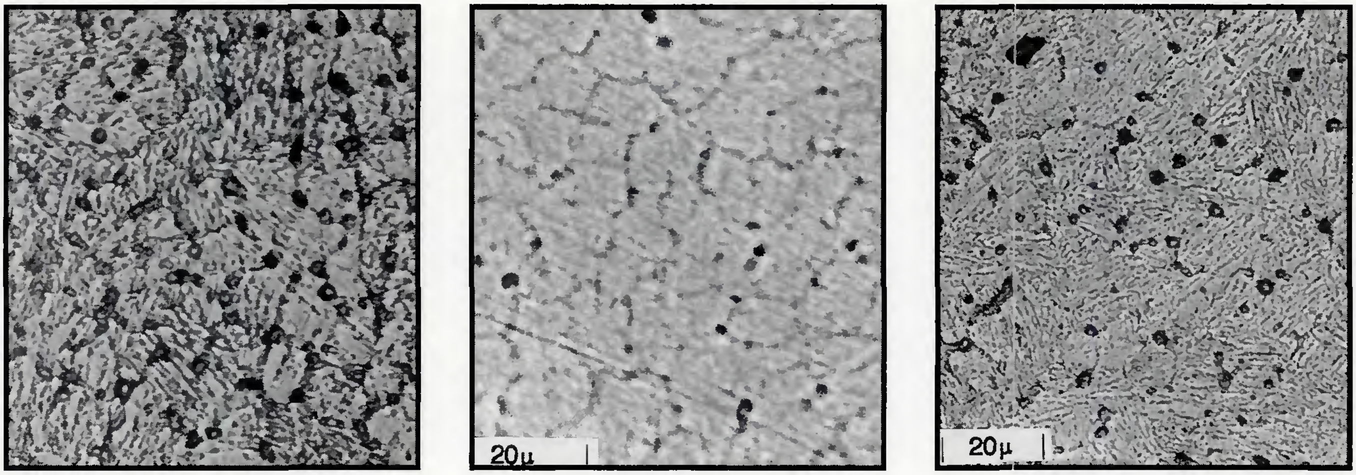

A B C

Fig. 3 — End-on dendrite morphologies for the 0.15C-1.5Mn steel spot welds. A — 0.8-mm-thick sample; B — nominally 1.25-mm-thick sample; C — nominally 2.0-mm-thick sample.

underlying transformed structure is difficult to observe. This is an indication of why this etchant was used; there is a strong tendency to etch even small variations in composition, rather than structural heterogeneities in the steel.

End-on views of the solidification structure for the three gauges of 0.10C-1Mn steel are presented in Fig. 2. Again, in order to adequately reveal the structure, SEM was used. These solidification structures differ from those observed in the 0.05C-0.3Mn steel in two major respects. First, the apparent degree of residual segregation was much greater. This was evident both from the fact that the dendrite structure was much easier to reveal on etching, and the appearance of "etch pits" located at dendrite triple points. These etch pits are undoubtedly the result of segregated C, which is preferentially attacked by the picric acid during etching. The second feature which distinguishes these results from those for the 0.05C-0.3 Mn steel is the scale of the solidification structure. In this case, the scale of the structure was great enough that it could be revealed at half the magnification.

Otherwise, the results are quite similar to those presented for the 0.05C-0.3Mn steel. Again, there is an apparent increase in the scale of the solidification structure with increasing gauge of the steel. Also, preferential etching of the solidification structure apparently has again obscured much of the underlying microstructure.

End-on views of the solidification structures for the three gauges of the 0.15C-1.5Mn steel are presented in Fig. 3. In this case, the primary dendrite spacings were so large and the degree of etching so pronounced, that optical microscopy could be used. In optimizing the microscope to reveal the primary dendrite structure, it was found useful to completely close down the aperture, and slightly deviate from proper focus. By defocusing the microscope, the "valleys" associated with the interdendritic regions could be resolved. However, this often reduced the overall quality of the image — Fig. 3B.

Compared to the other two steels, the apparent degree of segregation is again greater. This is clear from the size and frequency of the etch pits and the well demarked lines indicating the boundaries of the individual dendrites or cells. The scale of the solidification structure is here also clearly greater than for the other two materials. As for the other two materials, observed cell or dendrite spacing clearly increased with increases in the gauge of the steel used.

Table 3 — Positions of the Polished Surfaces for Dendrite Spacings Evaluations, as Well as Local Calculated Solidification Conditions for Each Material and Gauge Studied in Part II

Steel	Gauge (mm)	Position (mm)	Fract.	G (C/mm)	R (mm/s)	G × R (C/mm)	G × $R^{1/2}$ (C/mm × s)
0.5C-0.3Mn	0.79	0.53	0.25	750	13.57	10,200	2760
0.5C-0.3Mn	1.22	0.94	0.178	470	8.49	3990	1370
0.5C-0.3Mn	1.91	1.27	0.275	372	6.62	2460	957
0.10C-1Mn	0.74	0.46	0.28	854	15.48	13,200	6660
0.10C-1Mn	1.27	1.02	0.13	445	8.04	3580	1260
0.10C-1Mn	1.98	1.57	0.114	317	5.38	1700	735
0.15C-1.5Mn	0.89	0.66	0.257	635	11.42	7250	2150
0.15C-1.5Mn	1.45	0.91	0.321	495	8.79	4350	1470
0.15C-1.5Mn	2.13	1.70	0.107	278	5.03	1400	623

Measurements of Primary Dendrite Spacings

In this work, an averaged primary dendrite spacing was estimated from each micrograph. The basic approach for producing these estimates is shown in Fig. 4. Basically, the assumption is made that the dendrites, end-on, are configured in a two-dimensional closed-packed array. With this assumption, the average primary dendrite spacing (D) over the micrograph can be estimated from the measured area of the micrograph (A_{meas}), the number of dendrites in the micrograph (N) and the magnification of the micrograph (MAG), using the following equation:

$$d = \left(\frac{2}{\sqrt{3}} \times \frac{A_{meas}}{N \times MAG^2} \right)^{\frac{1}{2}} \tag{1}$$

As described above, the actual conditions governing solidification vary significantly with position in the weld. As such, the actual locations of the planes of polish used to measure these primary dendrite spacings must be documented for correlation with the estimated solidification conditions. This has been done for each of the metallographic samples and tabulated as the fractional position back into the sheet in Table 3.

Estimates of the primary dendrite spacings made from the micrographs of the three gauges of 0.05C-0.3Mn steel are presented in Table 4. Included on this table is the gauge of the steel, the measured area of the micrograph, the magni-

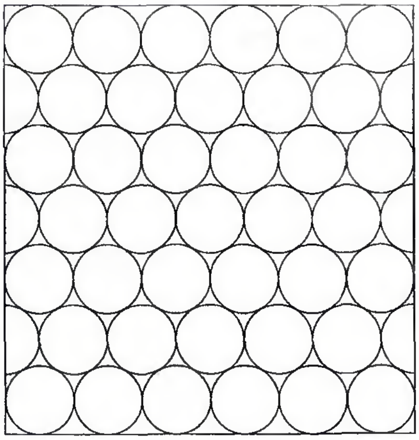

d = Primary Dendrite Spacing

Ameas = Measured Area of the Micrograph

N = Number of Primary Dendrites in the Micrograph

MAG = Magnification of the Micrograraph

$$d = \left(\frac{2}{\sqrt{3}} * \frac{Ameas}{N * MAG^2} \right)^{1/2}$$

Fig. 4 — Method of estimating primary dendrite spacings from the micrographs taken in this study.

fication of the micrograph, the number of dendrites counted in the micrograph and the estimated dendrite spacing. As described above, each micrograph was capable of yielding one estimate of the primary dendrite spacing. Therefore, in order to provide some assessment of reproducibility, a minimum of five micrographs were used to characterize each metallographic sample. This, in turn, yielded five separate estimates of the dendrite spacing.

The individual sets of primary dendrite spacings measurements for each gauge of the 0.05C-0.3Mn steel are quite consistent. Spacings for the 0.8-mm material range from 4.42 to 4.62 μm, those for the 1.25-mm steel range from 6.15 to 7.00 μm, and those for the heavy gauge of steel range from 8.23 to 8.83 μm. The dependence of gauge can also be seen, with spacings in the heavier gauge steel nearly double those in the lighter gauge material.

Estimated primary dendrite spacings for the three gauges of 0.10C-1Mn steel are presented in Table 5. Again, in order to provide some estimate or reproducibility, a minimum of five independent micrographs were used to estimate the dendrite spacing for each sample. Again, the estimates of primary dendrite spacing from a specific sample were relatively consistent with spacings increasing as a function of base metal thickness. Estimated spacings for the 0.8-mm-thick material ranged from 3.82 to 4.44 μm, those for the 1.25-mm-thick material ranged from 6.55 to 7.05 μm and those for the 2.0-mm material ranged from

Table 4 — Primary Dendrite Spacings Measurements for the 0.5C-0.3Mn Steel

Gauge (mm)	Position (mm)	Area (mm^2)	Magnification	N	d (μm)
0.79	0.53	6480	3000	60	4.42
0.79	0.53	6480	3000	58	4.50
0.79	0.53	6480	3000	55	4.62
0.79	0.53	6480	3000	61	4.39
0.79	0.53	6480	3000	59	4.46
1.22	0.94	6480	2000	65	6.38
1.22	0.94	6480	2000	54	7.00
1.22	0.94	6480	2000	70	6.15
1.22	0.94	6480	2000	55	6.94
1.22	0.94	6480	2000	65	6.38
1.91	1.27	6480	1600	53	8.83
1.91	1.27	6480	1600	57	8.52
1.91	1.27	6480	1600	55	8.67
1.91	1.27	6480	1600	61	8.23
1.91	1.27	6480	1600	60	8.30
1.91	1.27	6480	1600	54	8.75

Table 5 — Primary Dendrite Spacings Measurements for the 0.10C-1Mn Steel

Gauge (mm)	Position (mm)	Area (mm^2)	Magnification	N	d (μm)
0.74	0.46	3878	3000	42	4.09
0.74	0.46	4023	3000	38	4.38
0.74	0.46	2470	3000	37	3.82
0.74	0.46	5280	3000	56	4.13
0.74	0.46	4788	3000	44	4.44
1.27	1.02	5200	1500	76	7.05
1.27	1.02	6003	1500	95	6.77
1.27	1.02	3969	1500	64	6.71
1.27	1.02	5712	1500	90	6.78
1.27	1.02	4574	1500	77	6.57
1.27	1.02	3489	1500	59	6.55
1.98	1.57	6480	1500	75	7.42
1.98	1.57	6480	1500	55	9.25
1.98	1.57	6480	1500	57	9.08
1.98	1.57	6480	1500	54	9.33
1.98	1.57	6480	1500	64	8.57

Table 6 — Primary Dendrite Spacings Measurements for the 0.15C-1.5Mn Steel

Gauge (mm)	Position (mm)	Area (mm^2)	Magnification	N	d (μm)
0.89	0.66	6935	1520	109	5.64
0.89	0.66	6935	1520	85	6.39
0.89	0.66	6935	1520	93	6.10
0.89	0.66	6935	1520	90	6.21
0.89	0.66	6935	1520	86	6.35
0.91	0.91	6935	1050	63	10.73
0.91	0.91	6935	1050	79	9.59
0.91	0.91	6935	1050	70	10.19
0.91	0.91	6935	1050	67	10.41
0.91	0.91	6935	1050	91	8.93
1.91	1.70	6935	750	56	15.94
1.70	1.70	6935	750	71	14.16
1.70	1.70	6935	750	71	14.16
1.70	1.70	6935	750	66	14.69
1.70	1.70	6935	750	62	15.15
1.70	1.70	6935	750	61	15.28

7.42 to 9.33 μm. In this last case, with the exception of the single observation of 7.42 μm, the spacings were relatively more consistent, ranging only from 8.57 to 9.33 μm.

In general, the spacings (for specific gauges of steel) were greater for the 0.1C-1Mn steel than for the 0.05C-0.3Mn steel, though there was considerable overlap. This was not the case only for the nominally 0.8-mm samples, where the 0.1C-1Mn steel had an average spacing of about 4.2 μm, compared to an average spacing of 4.5 μm for the 0.05C-0.3Mn steel. This apparent discrepancy is probably due to a slight gauge variation between the two steels (about 0.8 mm for the 0.05C-0.3Mn steel compared to about 0.7 mm for the 0.1C-1Mn steel) as well as the apparent deeper section into the sheet on the 0.1C-1Mn steel (shown in Table 3).

Estimated primary dendrite spacings for the three gauges of the 0.15C-1.5Mn steel are presented in Table 6. As for the other steels, a minimum of five micrographs per sample were used to estimate primary dendrite spacings. This again provided some estimate of the reproducibility of the estimate. As in the previous cases, estimated dendrite spacings appeared to increase monotonically with increases in steel gauge. Also, the individual estimates were quite consistent. The ranges of these estimates included 5.64 to 6.39 μm for the 0.8-mm steel, 8.93 to 10.73 μm for the 1.25-mm steel and 14.16 to 15.94 μm for the 2.0-mm steel.

Estimated primary dendrite spacings for this material are about 50% greater than for the other two materials. This appears to be true for each of the three thicknesses of steel studied. There may be two contributing factors to this. First, the steel is unquestionably richer in composition, and based on Equations 2 and 3 in Part I of this study, this will lead to greater dendrite spacings. In addition, however, the actual thicknesses of the materials used were somewhat thicker for each of the three gauge classifications. This, as is clear from the results presented above, also leads to larger primary dendrite spacings.

Discussion

Relationships between Primary Dendrite Spacings and Solidification Conditions for the Various Steels

As described above, dendrite spacings are typically correlated with solidification conditions (G and R) in some sort of power relationship. To understand the relationships between primary dendrite spacings and solidification conditions for each of the steels studied, results are presented both as a function of G x R and G x $R^{1/2}$ on log-log plots. Regression analyses were done in all cases both to assess the quality of fit, and provide a quantitative estimate of the governing power relationships.

Log-log plots showing the relationships between the primary dendrite spacing and the two groupings of solidifica-

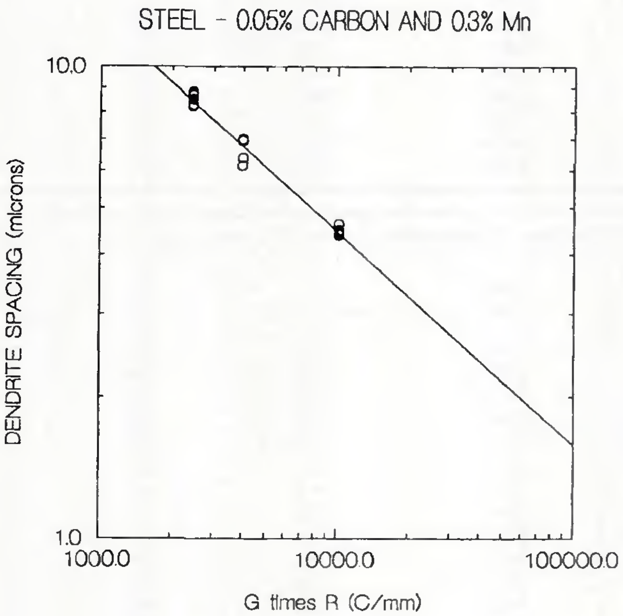

Fig. 5 — Variation in primary dendrite spacings for the 0.05C-0.3Mn steel as a function of G x R.

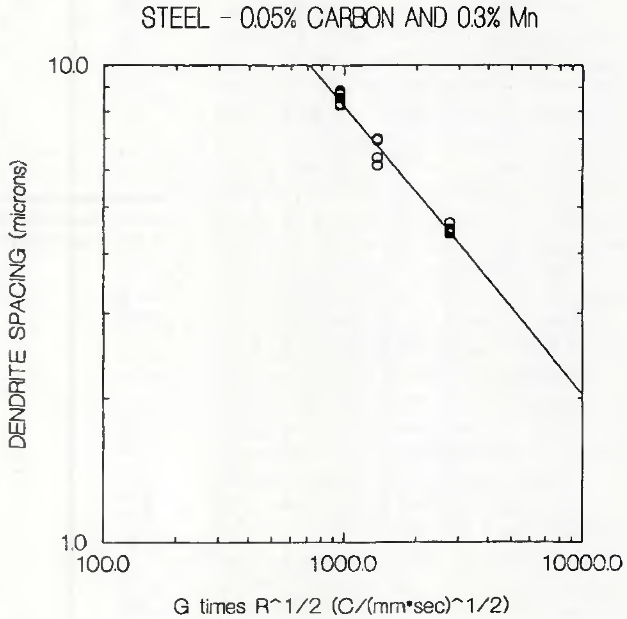

Fig. 6 — Variation in primary dendrite spacings for the 0.05C-0.3Mn steel as a function of G x $R^{1/2}$.

Table 7 — Regression Analyses of Primary Dendrite Spacings as a Function of G × R and G × $R^{1/2}$ for the 0.5C-0.3Mn Steels

	G × R	G × $R^{1/2}$
Exponent	−0.45	−0.60
Pre-exponent	282	532
R^2	97.8%	97.8%
F	624	618
Standard Error	0.285 μ	0.235 μ
Degrees of Freedom	15	15

(Results are for dendrite spacings measured in μm, G measured in °C/mm and R in mm/s.)

Table 8 — Regression Analyses of the Primary Dendrite Spacings as a Function of G × R and G × $R^{1/2}$ for the 0.1C-1.0Mn Steels

	G × R	G × $R^{1/2}$
Exponent	−0.36	−0.32
Pre-exponent	128	70.2
R^2	96.3%	94.9%
F	360	263
Standard Error	0.441 μ	0.521 μ
Degrees of Freedom	15	15

(Results are for dendrite spacings measured in μm, G measured in °C/mm and R in mm/s.)

tion conditions (G x R and G x $R^{1/2}$) are presented in Figs. 5 and 6. Included on these plots are regressed linear fits indicative of a power relationship. In both cases, a high degree of linearity is apparent. In fact, from these results, power relationships with both G x R and G x $R^{1/2}$ appear equally applicable. This difficulty in identifying differences between the two relationships is not surprising. Apparently, the change in the exponent on the solidification rate (R) is not a significant enough factor to appreciably affect the relationship on a log-log plot.

The accompanying regression analyses for these plots are presented in Table 7. As suggested from the plots presented above, the fits are very good, with R^2 values of almost 98%. Interestingly, both fits show virtually identical values for the three estimators of fit (R^2, error of the Y estimate and F statistic), again showing the difficulty in assessing the preferred predicting relationship. The actual predicted relationships from these fits are as follows:

As a function of G x R:

$$d = 282 \times (G \times R)^{-0.45} \qquad (2)$$

As a function of G x $R^{1/2}$:

$$d = 532 \times \left(G \times R^{\frac{1}{2}} \right)^{-0.60} \qquad (3)$$

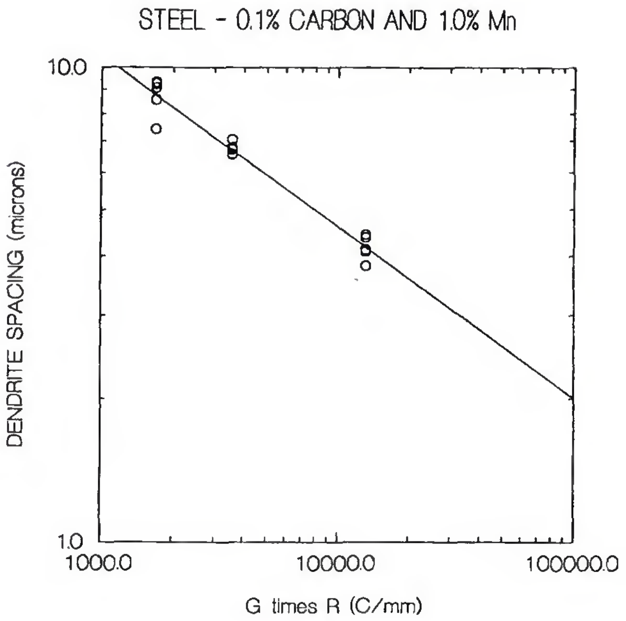

Fig. 7 — Variation in primary dendrite spacings for the 0.1C-1Mn steel as a function of G x R.

where d is in microns, G is in °C/mm and R is in mm/s. Most interesting to note are the estimated exponents on these relationships. In Equation 2, a value of 0.45 is estimated. This is very close to the exponents estimated in other works (Refs. 8–10). In Equation 3, an exponent of 0.60 is estimated. This compares very favorably with the value of ½ suggested by both the Hunt and Kurz-Fisher relationships described in Part I.

Log-log plots graphically showing the relationships between the primary dendrite spacings and the two groupings of solidification conditions are presented in Figs. 7 and 8. Again, included on these plots are the regression lines representing the best fit power expression. As with the 0.05C-0.3Mn steel results, the data appear to be well fit by both groupings of solidification conditions. Details of the regression analyses are presented in Table 8. Again, correlations for the two sets of groupings are similar in all major statistics (R^2, error of the Y estimate and F value). There is some indication that the G x R grouping may provide a better fit, but the difference is not considered significant.

Estimated power relationships based on the regression analyses for the two groupings are as follows:

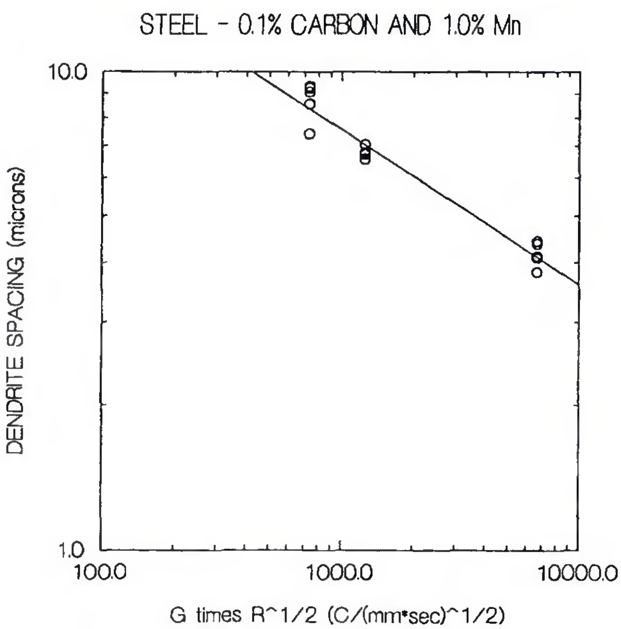

Fig. 8 — Variation in primary dendrite spacings for the 0.1C-1Mn steel as a function of G x $R^{1/2}$.

Table 9 — Regression Analyses of Primary Dendrite Spacings as a Function of G × R and G × $R^{1/2}$ for the 0.15C-1.5Mn Steels

	G × R	G × $R^{1/2}$
Exponent	−0.51	−0.67
Pre-exponent	603	1150
R^2	92.3%	92.2%
F	181	177
Standard Error	0.995 μ	1.02 μ
Degrees of Freedom	16	16

(Results are for dendrite spacings measured in μm, G measured in °C/mm and R in mm/s.)

Table 10 — Freezing Ranges (Δt_O) of Binary Fe-X Alloys, Where X Is the Alloying Addition of Interest, of Compositions Observed in the Alloys Used

Alloy Addition	Minimum Composition (%)	Maximum Composition (%)	Minimum ΔT_o (°C)	Maximum ΔT_o (°C)	ΔT_o/wt-%
C[a]	0.04	0.15	7.84	29.4	196
Mn[b]	0.31	1.51	0.54	2.63	1.74
S[b]	0.009	0.014	9.88	15.4	1104
P[a]	0.009	0.022	1.22	2.97	134.6
Si[a]	0.14	0.33	0.60	1.42	4.32

(a) Data estimated from phase diagrams in Ref. 14.
(b) Data estimated from phase diagrams in Ref. 15.

As a function of G x R:

$$d = 128 \times (G \times R)^{-0.36} \tag{4}$$

As a function of G x $R^{1/2}$:

$$d = 70.2 \times \left(G \times R^{\frac{1}{2}} \right)^{-0.32} \tag{5}$$

where d, G and R again have units of microns, °C/mm and mm/s, respectively. Interestingly, the exponents for these expressions are somewhat less than those for Equations 2 and 3 above. It is not known, however, whether this difference is significant. Still, the exponent of Equation 4 is within the range of values reported in the literature (Refs. 8–10). The exponent of Equation 5 is noticeably less than the value of ½ suggested by the Hunt and Kurz-Fisher expressions.

Log-log plots showing the relationships between primary dendrite spacings and the groupings of solidification conditions for the 0.15C-1.5Mn steel are presented in Figs. 9 and 10. As with the results for the other two steels, regression lines representing best fit power expressions are included on each figure. Again, both fits show a high degree of linearity, and it is difficult to distinguish differences in fit for the two groupings of solidification conditions. Regression analyses of the power expression fits are presented in Table 9. The degree of fit for these expressions is again quite similar, however, the fits are the poorest for the three steels studied. The reasons for this are not clear.

Based on these fits, the estimated power expressions are as follows:

As a function of G x R:

$$d = 603 \times (G \times R)^{-0.51} \tag{6}$$

As a function of G x $R^{1/2}$:

$$d = 1150 \times \left(G \times R^{\frac{1}{2}} \right)^{-0.67} \tag{7}$$

where d, G and R have the same units as previously described. In this case, the results were quite consistent with those for the 0.05C-0.3Mn steel. Exponents were roughly the same, and the pre-exponential terms were larger, presumably the effect of the richer composition. This latter aspect is suggested both from previous experimental work (Refs. 8–10), as well as the Hunt and Kurz-Fisher analyses.

Combined Effects of Composition and Solidification Conditions on the Primary Dendrite Spacings

Application of either the Hunt or Kurz-Fisher models, combined with the

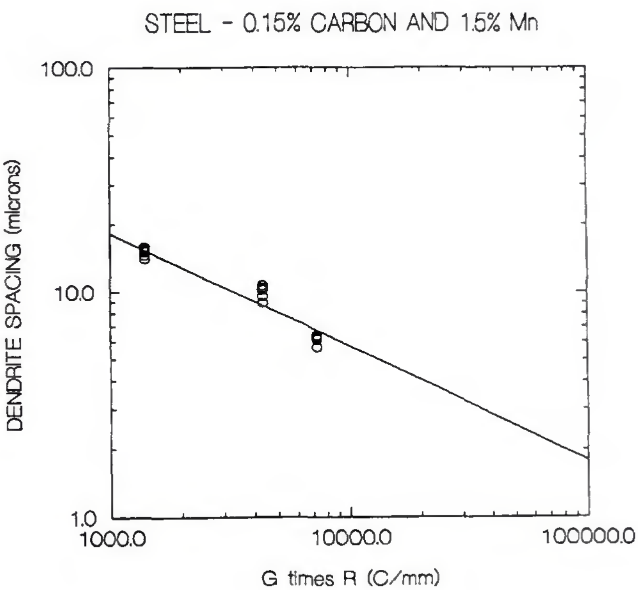

Fig. 9 — Variation in primary dendrite spacings for the 0.15C-1.5Mn steel as a function of G x R.

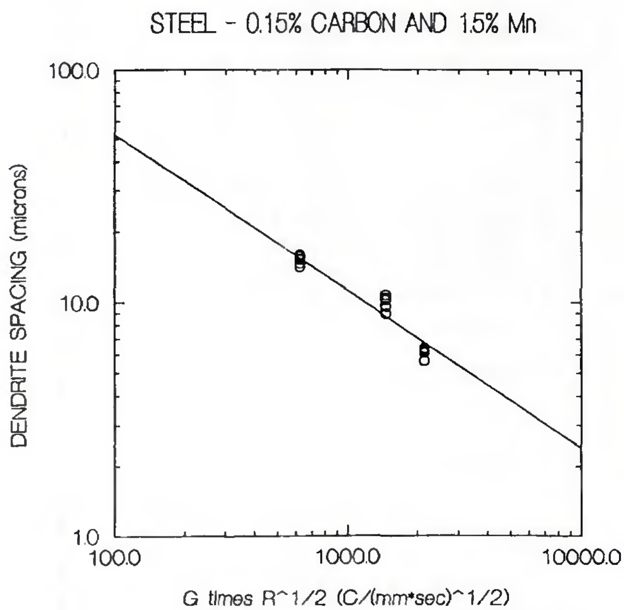

Fig. 10 — Variation in primary dendrite spacings for the 0.15C-1.5Mn steel as a function of G x $R^{1/2}$.

predicted solidification conditions from the numerical thermal model, provides an opportunity for also characterizing compositional effects on the primary dendrite spacing. Unfortunately, the Hunt and Kurz-Fisher models have been constructed only for binary systems. To apply these models to the steels studied here, the alloys must be considered as pseudo binary systems. This is a reasonable assumption, provided that the various alloy additions has a reasonably dominant influence on the development of the solidification structure.

Primary dendrite spacings are, in general terms, considered a function of the freezing range of the alloy, or ΔT_0. As such, an estimate of the effects of each of these additions on ΔT_0 will indicate their influence on the primary dendrite spacing. For the steels studied, the ranges of ΔT_0s associated with each alloy addition are listed in Table 10. ΔT_0s for carbon and sulfur are most dominant. However, given the low sulfur contents it is clear that the ΔT_0s for sulfur in these alloys are smaller and do not vary over the range of the ΔT_0s for carbon. In addition, the variation in ΔT_0s are random over the alloys studied, while those for carbon vary at defined levels over these materials studied. As such, the system here is considered to act as a series of pseudo binary Fe-C alloys with differing carbon contents.

Assuming that the steels studied here during solidification act as Fe-C binary alloys, primary dendrite spacings can be correlated by a combination of the estimated solidification conditions and the C content. Both the Hunt and Kurz-Fisher analyses then predict that the dendrite spacing can be expressed as a power function of the following lumped parameter:

$$\frac{c_o^{\frac{1}{2}}}{G \times R^{\frac{1}{2}}} \tag{8}$$

where c_o is the bulk C content of the steel.

A log-log plot showing the primary dendrite spacings measured in this work as a function of this parameter is presented in Fig. 11. This plot includes each of the roughly five estimations of primary dendrite spacings for each steel type and thickness. Linearity of the data on this plot indicates good adherence to a power relationship. These results indicate reasonably good fit to the power relationship over a variation of roughly an order of magnitude of the lumped parameter. This plot also indicates considerable overlap of the data for the individual steel types. The fitted power expression is also included on this plot for comparison.

The results of the regression analysis for the fitted power relationship are presented in Table 11. The statistics characterizing the degree of fit (R^2, standard estimate of the Y, and F statistic) all again indicate a relatively high level of correlation. The exact fitted relationship is as follows:

$$d = 447 \times \left(\frac{c_o^{\frac{1}{2}}}{G \times R^{\frac{1}{2}}} \right)^{0.48} \tag{9}$$

The most interesting characteristic of this equation is that the predicted exponent is extremely close to that by both the Hunt and Kurz-Fisher models. The results then appear to validate two assumptions made in this approach: that solidification conditions could be estimated with the one-dimensional thermal model, and the materials could be effectively treated as pseudo-binary Fe-C alloys.

Interestingly, what these results do not do is provide definite data for discerning the relative applicability of the Hunt vs. Kurz-Fisher models. To characterize this difference, it would be necessary to examine alloys whose solidification is dominated by additions with differing partition ratios (k). This, as mentioned previously, has been examined elsewhere for welds on Ti alloys (Ref. 11).

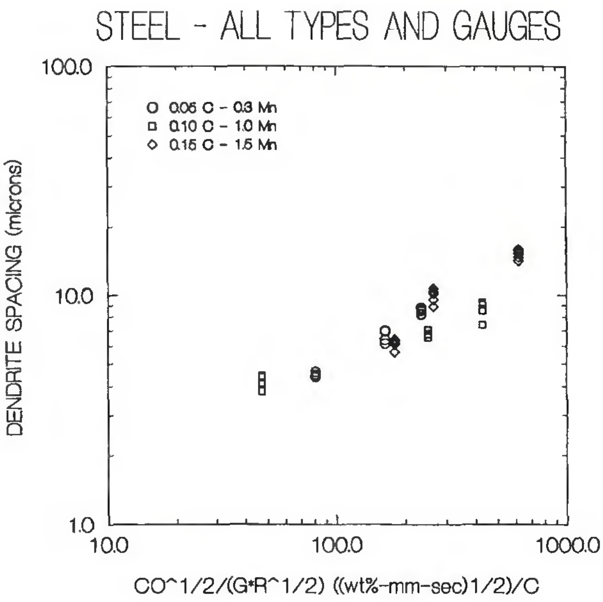

Fig. 11 — Variations in primary dendrite spacings for all the steels studied as a function of the lumped parameter $c_o^{1/2}/(G \times R)^{1/2}$.

Relationships between Primary Dendrite Spacings, Solidification Cracking and Hold Time Sensitivity

The results presented in this work suggest the following trends with respect to the primary dendrite spacing:

1) Higher C contents lead to coarser dendrite spacings in RSW.

2) RSW in thicker section steels have coarser dendrite spacings.

However, these do not correlate with the trends for solidification cracking and hold time sensitivity. Higher C contents do appear to lead to increased solidification cracking and hold time sensitivity; however, thicker section steels typically show reduced incidences of these types of problems. Clearly then, the primary dendrite spacing is, of itself, not a direct measure of cracking sensitivity.

Solidification cracking and hold time sensitivity are believed to be a complex interaction between the primary dendrite spacing and stress state active in the weld. Coarser primary dendrite spacings are considered detrimental to the cracking sensitivity for two reasons. First, the larger spacings infer a greater degree of segregation. The distance between the dendrite cores is greater, so based on a simple Sheil (Ref. 12) analysis, there will be a greater degree of solute buildup in the interdendritic regions. Second, a coarser dendrite spacing also reduces the degree of interdendritic surface area in

Table 11 — Regression Analyses of the Primary Dendrite Spacings as a Function of $C_o^{1/2}/(G \times R^{1/2})$ for all Steels

Exponent	0.48
Pre-exponent	447
R^2	85.3%
F	272
Standard Error	1.41 μ
Degrees of Freedom	48

(Results are for dendrite spacings measured in μm, G measured in °C/mm and R in mm/s.)

the weld. As such, there is a greater tendency to collect critical levels of liquid along the faying surface (final region to solidify) and back between the dendrites, resulting in cracking.

Certainly, increasing the primary dendrite spacing by increasing the C content has the effect of increasing cracking susceptibility. That a similar effect is not seen as the dendrite spacing increases with steel thickness is believed related to the developing stress state in the weld. Previous work (Ref. 13) has shown that cooling rates and thermal gradients in the workpiece increase markedly with reduced steel thicknesses. As the thermal gradients and cooling rates increase, so will the tendency for differential thermal contraction in the weld. It is believed that in the lighter gauge steels the solidified material simply contracts at an accelerated rate, leaving voids both at the weld centerline as well as back in between the dendrites. For the lighter gauge materials, it is believed these contraction effects swamp the benefits of a refined solidification structure, increasing the weld crack susceptibility. Clearly, to understand these effects will require more sophisticated modeling capable of characterizing these contractual stresses as well as the primary dendrite spacing.

Conclusions

In this work, primary dendrite spacings in resistance spot welds have been studied through a combination of numerical process modeling and existing structural development modeling. In a previous article (Part I), numerical thermal modeling of the resistance spot welding process was used to estimate solidification conditions in resistance spot welds. These solidification results were then used with existing closed-form primary dendrite spacings models to predict spacings in spot welds. In this paper, the modeling results were correlated with primary dendrite spacings measurements on three steels of progressively increasing C and Mn contents. Three thicknesses of each steel type were used. From this work, the following conclusions were drawn:

1) *Method of Estimating Primary Dendrite Spacings.* Primary dendrite spacings were estimated from micrographs taken end-on by assuming a closed packed distribution. This technique proved to be quite reproducible on multiple micrographs from the same sample.

2) *Variation in Primary Dendrite Spacings as a Function of Gauge.* Primary dendrite spacings were consistently found to increase with steel gauge for the three steel compositions under study.

3) *Variation in Primary Dendrite Spacings as a Function of Composition.* Steels of progressively higher C and Mn contents were found also to have progressively larger primary dendrite spacings.

4) *Estimation of Solidification Conditions for the Samples under Study.* Based on the initial geometry of the weld configuration, and degree of maximum nugget penetration, solidification conditions representative of the positions in the weld from which the primary dendrite spacings measurements were taken could be calculated.

5) *Primary Dendrite Spacings vs. $G \times R$ and $G \times R^{1/2}$.* Using the variation in gauge to provide the variation in solidification conditions, primary dendrite spacings were found to correlate very well with either $G \times R$ or $G \times R^{1/2}$ in a power relationship. This was true for all three compositions of steel studied. Estimates of the exponents in these power relationships were consistent with other works. It was not possible, however, to determine which relationship was more applicable for predicting primary dendrite arm spacings.

6) *Treatment of These Alloys as a Pseudo Fe-C Binary System for Solidification.* Based on estimates of the material-dependent parameters in either the Hunt or Kurz-Fisher models ($k \Delta T_o$ or $\Delta T_o/k$, respectively), it was found that C was the dominant compositional variable affecting solidification. As such, the steels used in this study were considered as pseudo-binary Fe-C alloys for examining solidification characteristics.

7) *Primary Dendrite Spacings vs. the Lumped Parameter $c_o^{1/2} /(G \times R^{1/2})$.* Using the pseudo-binary approximation for these steels, primary dendrite spacings results for all nine variations of steel (three gauges, three compositions) could be fit to the same power relationship. This relationship correlates the primary dendrite spacing with a lumped parameter $c_o^{1/2} /(G \times R^{1/2})$. This relationship is predicted from both the Hunt and Kurz-Fisher models. A high degree of fit was noted, and the predicted exponent was nearly identical to that suggested by either model.

8) *Relationships between the Primary Dendrite Spacing, Solidification Cracking and Hold Time Sensitivity in Spot Welds.* Primary dendrite spacing as a function of gauge and composition did not vary in a way consistent with previous work on solidification cracking and hold time sensitivity. As such, the primary dendrite spacing can, of itself, not be considered an indicator of these problems. It is believed that solidification cracking and hold time sensitivity in spot welds is a function both of the primary dendrite spacing and the rate of thermal contraction of the solidified weld metal during solidification. Therefore, it is believed more detailed modeling, capable of predicting both primary dendrite spacings and thermal contraction effects will be required to detail solidification cracking and hold time sensitivity in resistance spot welds.

Acknowledgments

The author would like to thank the Inland Steel Co. under whose employ the bulk of this work was conducted. Also, to P.-H. Chang for his contributions. Discussions with A. Preban, R. Rivett and M. Kimchi are also acknowledged. Finally, the author would like to acknowledge Neal Saboff who conducted the bulk of the experimental work in this program.

References

1. Fine, T. E., and Fostini, R. V. 1979. Spot weldability of high strength, cold rolled steels. SAE Technical Paper 79005, SAE, Warrendale, Pa.

2. Sawhill, J. M., Jr., and Furr, S. T. 1984. Weldability considerations in the development of high strength sheet steels. *Welding Journal* 63(7):203-s to 212-s.

3. Goodman, S. R., and Domis, W. F. 1982. Effects of carbon, phosphorus and sulfur content on the tensile properties and spot weldability of high-strength cold-rolled sheet. SAE Technical Paper 820280, SAE, Warrendale, Pa.

4. Gould, J. E. 1985. Unpublished research, Inland Steel Company.

5. Baker, R. G., and Newman, R. P. 1969. Cracking in welds. *Metal Construction and British Welding Journal* 16(2):1–4.

6. Gould, J. E. 1994. Modeling primary dendrite arm spacings in resistance spot welds, part I — modeling studies. *Welding Journal* 73(4).

7. 1980. Ford Laboratory Test Methods, Schedule BA13-4.

8. Spittle, J. A., and Lloyd, D. M. 1979. Dendrite arm spacings in hypoeutectic Pb-Sb alloys directionally solidified under steady and nonsteady conditions. *Solidification and Casting of Metals,* conference proceedings, pp. 15–20.

9. Rohatgi, P. K., and Adams, C. M., Jr. 1967. Dendritic solidification of aluminum copper alloys. *Transactions of the Metallurgical Society of AIME,* 234(11):1737–1746.

10. Young, K. P., and Kirkwood, D. H. 1975. The dendrite arm spacings of aluminum copper alloys solidified under steady state conditions. *Metallurgical Transactions,* 6A(1):197–205.

11. Gould, J. E. 1983. Effect of composition and weld process on the structure of titanium-alloy welds. Ph.D. dissertation, Carnegie-Mellon University.

12. Flemings, M. C. 1974. *Solidification Processing,* McGraw Hill, New York, N.Y.

13. Gould, J. E. 1987. An examination of nugget development during spot welding, using both experimental and analytical techniques. *Welding Journal* 66(1):1-s to 10-s.

14. *Binary Alloy Phase Diagrams.* 1990. 2nd Ed., Vols. 1 and 2. ASM International Pubs., Materials Park, Ohio.

15. *Metals Handbook,* Vol. 8. 1974. 8th Ed., ASM Pubs., Materials Park, Ohio.